Heliyon

Received:
30 January 2019
Revised:
25 February 2019
Accepted:
15 April 2019

Cite as:
Akeem
Damilola Akinwekomi.
Microstructural
characterisation and corrosion
behaviour of microwave-
sintered magnesium alloy
AZ61/fly ash microspheres
syntactic foams.
Heliyon 5 (2019) e01531.
doi: 10.1016/j.heliyon.2019.
e01531

Microstructural characterisation and corrosion behaviour of microwave-sintered magnesium alloy AZ61/fly ash microspheres syntactic foams

Akeem Damilola Akinwekomi*

Department of Metallurgical and Materials Engineering, Federal University of Technology, PMB 704, Akure, Ondo State, Nigeria

* Corresponding author.

E-mail address: adakinwekomi@futa.edu.ng (A.D. Akinwekomi).

Abstract

Magnesium alloy AZ61/fly ash microspheres (FAMs) syntactic composite foams were synthesised via powder metallurgy and microwave (MW) sintering techniques. MW sintering was rapidly completed in 20 min and minimized the formation of brittle interfacial products. Effect of FAMs on the density, microstructure, and corrosion resistance of the alloy were investigated. FAMs were intact and fairly distributed in the microstructure of the foams. Corrosion behaviour in 3 wt.% sodium chloride solution showed that Tafel polarization curves shifted to lower current densities as the volume fraction of FAMs increased. This indicated that FAMs generally enhanced the corrosion resistance of the foams due to minimal galvanic interaction and reduction in the surface area of the material exposed to the corrosion medium. These results are significant and outline the enhancement of corrosion resistance of magnesium alloy AZ61 foams by using FAMs.

Keywords: Materials science, Metallurgical engineering

https://doi.org/10.1016/j.heliyon.2019.e01531

1. Introduction

Lightweight energy absorption materials are required in many engineering applications, such as in aerospace, automobile, and railway. Magnesium (Mg)-based foams exhibit low density, high specific strength and large compressive deformations, making them ideal materials for lightweight energy absorption applications [1, 2, 3]. Mg-based syntactic foams incorporate hollow ceramic particles, such as fly ash microspheres (FAMs), which form the closed-cell structure exhibited by such syntactic foams. Unlike other closed-cell foams that are synthesised by the aid of gas-releasing agents, syntactic foams are characterised by higher moduli and strengths, due to the support offered by the shells of the fly ash microspheres [1, 4].

Mg-based syntactic foams fabricated via the powder metallurgy (PM) processing technique require one or more sintering stages, which can be accomplished via conventional and non-conventional sintering approaches. Conventional sintering involves extended sintering time of several hours and this increases the tendency for the formation of brittle interfacial products between FAMs and the matrix [1, 5]. These products adversely affect strength [6] and may probably exacerbate corrosion problems. Thus, microwave (MW) sintering has emerged as an important non-conventional alternative. MW sintering is a rapid sintering process where heating occurs due to the interaction between electromagnetic waves and the dipoles in a material. This heating process is rapid and significantly reduces energy consumption and processing time [7, 8]. As a result, MW sintering can minimize unwanted interfacial reactions between FA particles and the matrix.

Mg-based syntactic foams have high potentials to be used in the automotive and aerospace industries. Although many studies have been dedicated to investigating some of their mechanical [1, 9, 10] and electromagnetic shielding properties [11], studies on their corrosion behaviour are grossly lacking. In the past, some authors have investigated the corrosion behaviour of some Mg-based foams [2, 12], albeit with conflicting conclusions. Using sodium chloride (NaCl) solutions, Xia et al. [12] show that closed-cell AZ31 foams have higher corrosion resistance than the base alloy. The authors report that AZ31 foams have finer and continuous corrosion precipitates that are distributed along the grain boundaries, thus limiting corrosion to within the grain boundaries. On the contrary, porosity is reported to exacerbate the corrosion of Mg foams in NaCl and phosphate buffered saline (PBS) solutions [2].

Studies on the corrosion behaviour of Mg-based syntactic foams are limited [13, 14]. In a study focusing on Mg alloy AZ91D syntactic foams containing hollow glass microspheres (HGM), the authors report that the syntactic foam samples show improved corrosion resistance in 3.5% sodium chloride (NaCl) solution compared with the base alloy. This is attributed to the presence of HGMs, which reduce the

https://doi.org/10.1016/j.heliyon.2019.e01531

overall surface area of the matrix [14]. Similarly, silica nanospheres are reported to enhance the corrosion resistance of Mg in both Hank's buffered saline and PBS solutions [13].

Mg-based syntactic foams have potentials to be used in some structural applications where they may be exposed to some corrosive media. These few studies [13, 14] are insufficient to adequately establish their corrosion behaviour. Therefore, more studies are required to provide further information and knowledge on their corrosion behaviour, especially for those prepared via powder metallurgy (PM) approach. The present study, therefore, seeks to contribute to the body of knowledge in this field and elucidate the effect of fly ash microspheres on the microstructure and corrosion behaviour of Mg alloy AZ61/fly ash syntactic foams. The foams are synthesised via PM and microwave (MW) sintering techniques. MW sintering is shown to be rapid with the attendant advantage of minimising the formation of brittle interfacial products. The corrosive medium is 3.5 wt.% NaCl solution and potentiodynamic polarisation technique is used to determine the corrosion properties of the samples. Corroded surfaces are further characterised by a scanning electron microscope (SEM).

2. Materials and methods

The matrix material was AZ61 Mg alloy powder (~50 μm; Tangshan Weihao Magnesium Powder Co., Ltd., China) while fly ash microspheres, FAMs (Ø 100−250 μm; Hebei DFL Minmet Refractories Corp, China) were used as space holders for forming the closed cell structure. Fig. 1 shows the SEM images of FAMs and AZ61 powder. The FAMs are mostly spherical in shape, although a few broken and irregularly shaped ones could be seen in the micrograph (see the arrows in Fig. 1(a)). AZ61, on the other hand, appeared flaky in Fig. 1(b). FAMs are chemically made up of alumino-silicate minerals, comprising Al_2O_3 (33−38 %), SiO_2 (56−62 %), Fe_2O_3 (2−4 %), and some other metallic oxides in minor proportion [1]. The density of FAMs was 0.70 g/cm^3 and were pre-treated with 1 M KOH

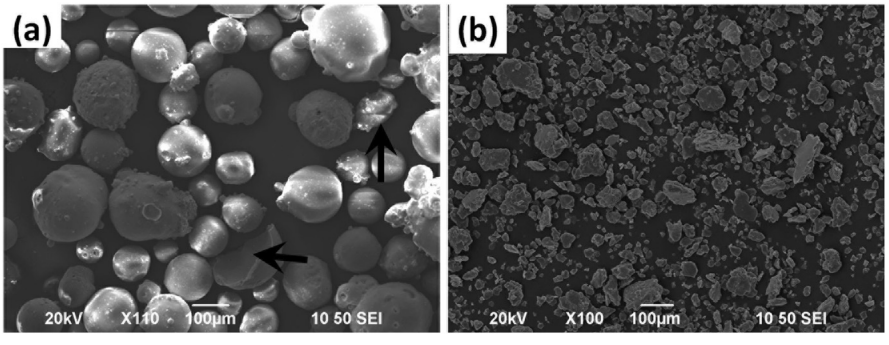

Fig. 1. SEM images of (a) fly ash microspheres (b) AZ61 powder.

https://doi.org/10.1016/j.heliyon.2019.e01531

solution for 1 h at 100 °C in. After pre-treatment, FAMs were washed with DI water until neutral pH and dried for 2 h at 100 °C. AZ61 powder was mixed with 20, 30, and 40 vol.% FAMs using a planetary mechanical mixer for 5 min and later uniaxially pressed to cylindrical specimens at 120 MPa for 2 min. The samples were later sintered for 20 min at a temperature of 550 °C in a commercial 2.45 GHz HAMiLab-HV3 high vacuum multimode MW furnace (SYNOTHERM Corporation, China). More details about the sintering set up can be found in a previous report [1]. The densities of the sintered samples are determined by mass-volume relationship.

X-ray diffraction (XRD) analysis of the sintered samples were done to determine the intermetallic phases present. This was done at a scanning speed of 4°/min on a Rigaku SmartLab XRD machine using a Cu Kα radiation ($\lambda = 1.54056$ Å).

For corrosion test specimens, samples were cut into rectangular shapes using an electrical discharge machine (Acro Star II WEDM, Acro Machinery & Electric Co., Ltd., Taiwan) and embedded in cold-setting epoxy resins by exposing a rectangular area of ~ 0.35 cm^2. The exposed surface was mechanically ground with silicon carbide (SiC) paper up to a grit of 1200 using 1 μm diamond paste and finished with 0.25 μm diamond paste. The samples were ultrasonically cleaned in 95% acetone.

Electrochemical polarisation tests were performed on a Parstat 2263 Advanced Electrochemical System (Princeton Advanced Research) The polarisation test was performed in a corrosion cell containing 150 ml of 3 wt.% NaCl solution (pH = 7.25) using a standard three-electrode configuration. Reference electrode was the saturated calomel electrode (SCE), counter electrode was graphite, while the working electrode was the test specimen. The potential was scanned from −2600 to −800 mV at a scanning rate of 5 mV/s. All the tests were carried out at room temperature (23 ± 2 °C). After the corrosion tests, microstructural examination of the corroded surfaces was undertaken using a scanning electron microscope (SEM; JEOL JSM-6490) equipped with an Oxford Instrument energy dispersive X-ray (EDX) facility.

3. Results and discussion

AZ61/FAM syntactic foams are successfully fabricated via PM approach and rapidly sintered in a MW furnace in 20 min. This rapid sintering technique is significantly shorter than the conventional sintering durations reported in some previous studies. For instance, conventional sintering durations of 120 min [15] and 360 min [16] are reported for open-cell Mg-based foams. Compared to these two studies, MW sintering time reported in this present study is significantly shorter by ~17% and ~6%, respectively. This reduced sintering time is advantageous in reducing energy consumption, increasing production rate, and minimizing the formation of undesirable interfacial phases. A study reports a 17 min MW sintering time for Mg/FAM syntactic foam [10]. However, the sintering temperature is 640 °C, about 14% higher than

https://doi.org/10.1016/j.heliyon.2019.e01531

Table 1. Comparison of the theoretical and sintered densities of AZ61 and AZ61/FAMs syntactic foams.

Sample	Theoretical density (g/cm^3)	Sintered density (g/cm^3)	% Reduction in density[a]	Porosity (%)[a]
AZ61	1.81	1.58 ± 0.03	-	-
AZ61/20% FAMs	1.59	1.21 ± 0.01	23.18	23.18
AZ61/30% FAMs	1.48	1.30 ± 0.03	17.83	17.83
AZ61/40% FAMs	1.37	1.26 ± 0.04	20.28	20.28

[a] As compared with the density of sintered AZ61.

the temperature utilised in the present research. Although a high sintering temperature enhances diffusion, it nevertheless increases the propensity for the oxidation of Mg [3, 16] and reaction with FAMs.

Table 1 shows the densities of sintered AZ61 and AZ61/FAMs syntactic foams. The incorporation of FAMs into AZ61 matrix gives rise to a reduction in the sintered densities of the syntactic foams. The lowest density of 1.21 g/cm^3 is exhibited by AZ61/20% FAMs, which translates to a density reduction of about 23%, when compared with the density of sintered AZ61. Of all the syntactic foams, the highest sintered density is 1.30 g/cm^3 (AZ61/30% FAMs), which is ~18% lighter than sintered AZ61. Similar density reduction have been reported in similar Mg-based matrices incorporating FAMs [1, 10].

Porosity of the samples is evaluated from the expression [17] $1-(\rho_{sin}/\rho_{th})$; where ρ_{sin} and ρ_{th} are the sintered density of the sample and its corresponding theoretical density, respectively. It is expected that AZ61/40% FAMs should exhibit a lower density (or a higher porosity) than AZ61/20%, but the reverse is observed in Table 1. This may be due to the crushing of some FAMs during the compaction of green samples (see Fig. 2). As FAMs are crushed and compacted, their density approach that of a fully dense material and may contribute to increment in the density (or reduction in porosity) of the syntactic foam samples. This is similar to the reports in some previous studies [9, 10]. In melt-processed syntactic foams, this discrepancy is attributed to the filling of FAMs by molten metal during processing [18].

It can also be observed from Table 1 that the sintered densities of the syntactic foams are lower than their theoretical densities. This can be attributed to the low compaction pressure utilized in forming the foams. PM processing requires a high compaction pressure to densify PM products and minimize interparticle porosity. However, this will damage the hollow FAMs and defeat the goal of realizing lightweight syntactic foams. Therefore, there is a trade-off between achieving a dense material (i.e. minimizing interparticle porosity) and preserving the structural integrity of the FAMs. This observation and postulation are in accordance with findings from some earlier studies [1, 19].

https://doi.org/10.1016/j.heliyon.2019.e01531

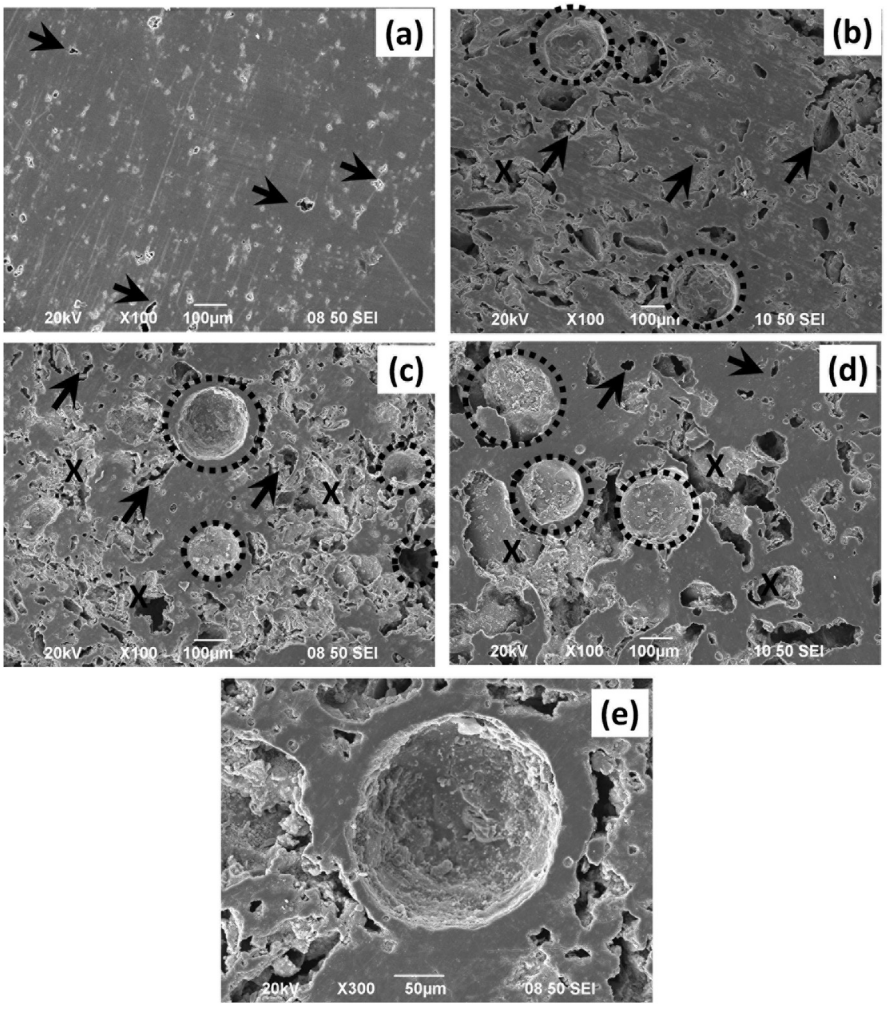

Fig. 2. SEM micrographs of the surfaces of (a) dense AZ61 (b) 20% FAMs syntactic foam (c) 30% FAMs syntactic foam (d) 40% FAMs syntactic foam (e) magnified image of the interfacial region between a FAM and AZ61 matrix.

SEM micrographs of sintered AZ61 and AZ61/FAMs syntactic foam samples are shown in Fig. 2. The surface of AZ61 in Fig. 2(a) shows a few interparticle porosity, as indicated by the black arrows. Some FAMs are enclosed within the black, dotted circles, while crushed or distorted FAMs are marked with an "X". It is evident from the micrographs that a large number of the FAMs are intact after the sintering process and their spherical shape (as shown in Fig. 1(a)) are largely preserved. The crushed/distorted FAMs are believed to have come from the as-received FAMs (see arrow in Fig. 1(a)) while some may have been crushed during the compaction process of making the green samples. FAMs generally have thin shells, which are weak and susceptible to cracking and fracturing during the compaction of green samples. Similar features have been observed in some earlier studies on powder metallurgy processed

https://doi.org/10.1016/j.heliyon.2019.e01531

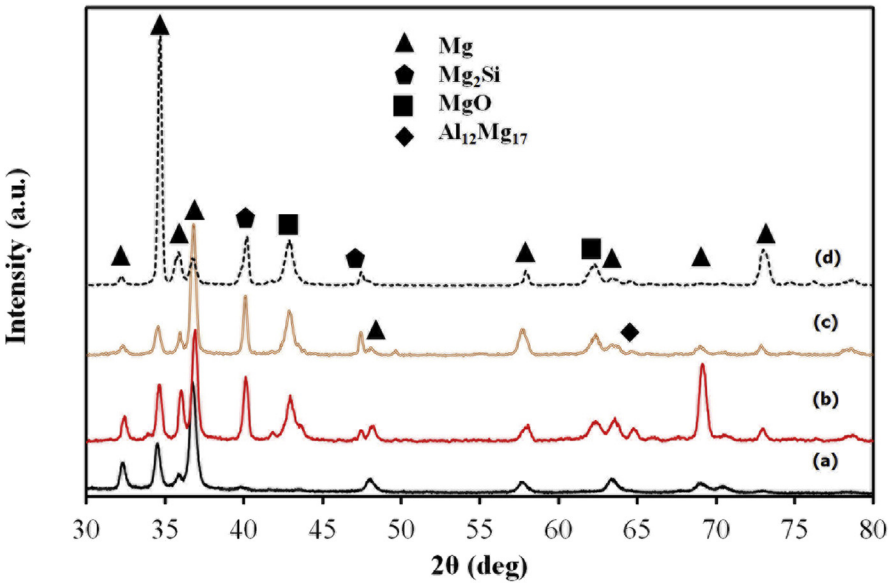

Fig. 3. XRD patterns of sintered (a) AZ61 (b) AZ61/20% FAMs (c) AZ61/30% FAMs (d) AZ61/40% FAMs.

syntactic foams [1, 5]. Other than FAMs, some interparticle pores, which are indicated by some arrows, are also present in the micrographs. These arise due to the low compaction pressure utilised in pressing the samples. On the other hand, an unoptimized compaction pressure will lead to significant damage of the FAMs.

X-ray diffraction patterns of AZ61 and AZ61/FAMs syntactic foams are shown in Fig. 3.

Prominent peaks of Mg are easily identified from the diffractogram. Other peaks indexed are MgO, Mg_2Si, and $Al_{12}Mg_{17}$. MgO and Mg_2Si are thought to be reaction products between Mg and the alumina (Al_2O_3) and silica (SiO_2) present in FAMs. MgO and Mg_2Si are formed according to the following reactions (Eqs. (1), (2), and (3)) as reported in Refs. [1, 20]:

$$3\ Mg + Al_2O_3 \rightarrow 3\ MgO + 2Al \quad (1)$$

$$2\ Mg + SiO_2 \rightarrow 2\ MgO + Si \quad (2)$$

$$2\ Mg + Si \rightarrow Mg_2Si \quad (3)$$

In Eq. (1), Mg reacts with Al_2O_3 (from FAMs) to yield MgO and Al. Simultaneously, Mg also reacts with SiO_2 (from FAMs) to form MgO and Si. A further reaction between Si and the excess Mg in the matrix gives rise to Mg_2Si, according to

https://doi.org/10.1016/j.heliyon.2019.e01531

Eq. (3). Despite that these reactions occurred, no discernible outgrowths are observed in the interface between FAMs and the AZ61 matrix, as shown in a typical high magnification micrograph of the interface in Fig. 3(d). This is in contrast with the observation reported in a previous study [20], wherein significant outgrowths of Mg_2Si could be seen at the interface. The result of the present investigation strongly suggests that the rapid microwave sintering process minimised these reactions and any Mg_2Si formed is not resolved at the magnification used for imaging the samples.

Polarisation curves of the samples are shown in Fig. 4. Typically, the cathodic portion of the polarisation curve is related to the evolution of hydrogen as water is reduced, while the anodic portion corresponds to the dissolution of Mg in aqueous solution. Furthermore, it is widely accepted that Tafel curves of materials that exhibit more positive corrosion potential (E_{corr}) and lower corrosion current density (i_{corr}) show enhanced corrosion resistance compared with materials that exhibit opposite behaviours [21]. It is noted that the curves are shifted to lower current densities as the volume fraction of FAMs increases in the syntactic foams. Pure AZ61 exhibit a current density of 2.86 μA/cm^2, which reduces to 2.79, 1.83, and 0.48 μA/cm^2 for 20%, 30%, and 40% FAMs, respectively. Similarly, the corrosion potentials (E_{corr}) generally follow the same trend. While the E_{corr} of AZ61 is −1462.04 mV, syntactic samples exhibited more positive values (−1412.60 and −1171.76 mV for 30% and 40% FAMs, respectively). Nevertheless, AZ61/20% FAMs syntactic sample shows an E_{corr} value of −1478.82, which is lower than that of AZ61. A summary of the polarization data is shown in Table 2.

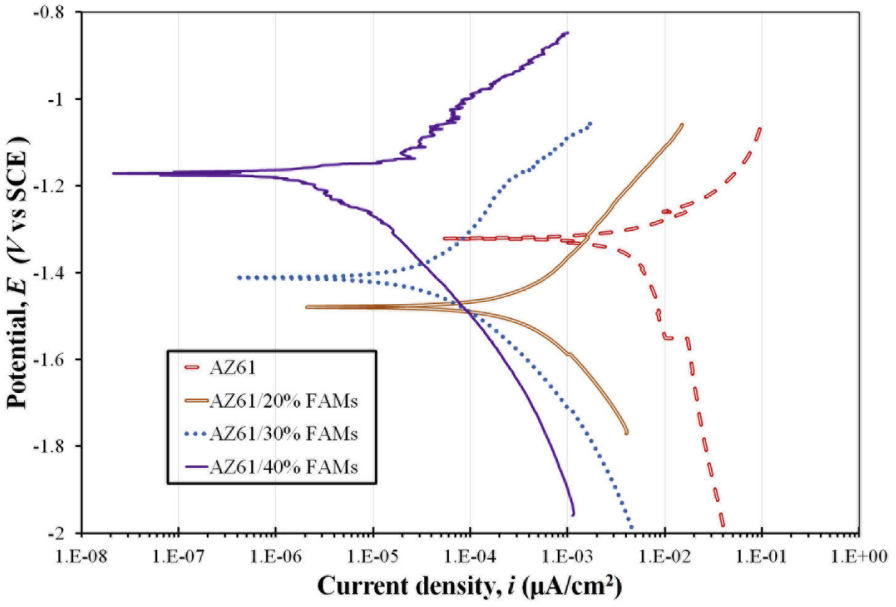

Fig. 4. Electrochemical polarization curves of AZ61 and AZ61/FAMs syntactic foams.

https://doi.org/10.1016/j.heliyon.2019.e01531

Table 2. Results from polarisation tests showing corrosion potential, current density, and corrosion rate for each sample.

Sample	E_{corr} (mV)	i_{corr} (μA/cm^2)	CR, corrosion rate (mm/yr)
AZ61	−1462.04	2.86	0.071
AZ61/20% FAMs	−1478.82	2.79	0.090
AZ61/30% FAMs	−1412.60	1.83	0.055
AZ61/40% FAMs	−1171.76	0.48	0.015

Corrosion rate (CR) tends to decrease with an increase in the volume fraction of FAMs, except for AZ61/20% FAMs syntactic foam, which has the highest corrosion rate of 0.09 mm/yr. This observation is consistent with the value of its corrosion current density. The CR value of pure AZ61 is 0.071 mm/yr, which further reduces to 0.055 and 0.015 mm/yr in syntactic foam samples with 30 and 40 vol.% FAMs. These observations suggest that FAMs generally enhance the corrosion resistance of the alloy. Although the results of some earlier studies indicate that the CR of Mg-based composites deteriorate when the reinforcement exhibit galvanic coupling with the matrix. Such reinforcements include graphene [22] and carbon nanotubes [23, 24]. However, FAMs are largely made up of non-conducting and insulating alumino-silicate minerals [25]. Thus, the CR of the syntactic foams are lower than that of pure AZ61 due to the absence of galvanic interaction between FAMs and AZ61 matrix [26] and reduction in the active matrix area (due to the presence of FAMs) exposed to the corrosion medium [14]. Moreover, this observation agrees with CR reported in some earlier studies on Mg alloy AZ91D/hollow glass syntactic foam samples [14], Mg reinforced with hollow silica nanospheres [13], and Mg reinforced with *in-situ* MgO and Mg-Zn intermetallics [21].

Fig. 5 shows the SEM micrographs of the surfaces of the corroded samples. In Fig. 5(a), the corroded surface of AZ61 shows extensive prominent outgrowths of whitish corrosion products (black, dotted oval shape). A larger magnification of this feature in Fig. 5(e) shows clear needle-like crystals and EDX analysis in Fig. 5(f) suggests that the crystals are mostly composed of elemental Mg and O. Thus, this corrosion product may be a mixture of MgO and $Mg(OH)_2$. MgO, on the other hand, can be further hydrated to form $Mg(OH)_2$ [21]. Hence, $Mg(OH)_2$ is regarded as the most common corrosion product on Mg matrix [26, 27]. According to Ref. [22], the formation of $Mg(OH)_2$ can be summarised as shown in Eqs. (4), (5), and (6):

$$Mg_{(s)} \rightarrow Mg_{(aq)}^{2+} + 2e^{-} \text{ (anodic reaction)} \quad (4)$$

$$2H_2O_{(aq)} + 2e^{-} \rightarrow H_2(g) + 2OH^{-}_{(aq)} \text{ (cathodic reaction)} \quad (5)$$

https://doi.org/10.1016/j.heliyon.2019.e01531

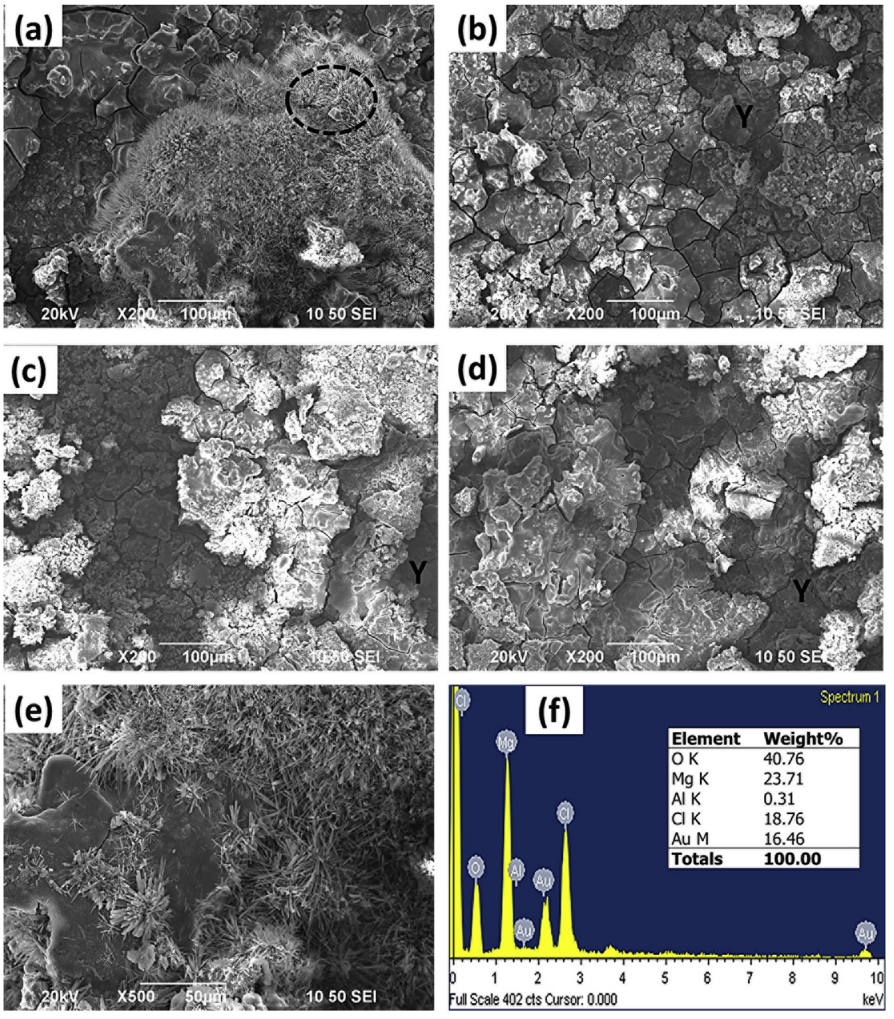

Fig. 5. SEM micrographs of corroded surfaces of (a) AZ61, (b) AZ61/20% FAMs, (c) AZ61/30% FAMs, (d) AZ61/40% FAMs; (e) magnified image of the portion enclosed in a dotted circle in (a), and (f) EDX analysis of (e).

$$Mg_{(aq)}^{2+} + 2OH_{(aq)}^{-} \rightarrow Mg(OH)_2 \text{ (corrosion product)} \quad (6)$$

Moreover, some cracks are visible from the micrograph in Fig. 5(a), however, heavy outgrowths of $Mg(OH)_2$ crystals appear to cover many of these cracks. Similar features can be seen in the micrographs of the syntactic foam samples in Fig. 5(b), (c), (d). However, $Mg(OH)_2$ crystals are less prominent in these micrographs as compared with Fig. 5(a) for AZ61. Unlike the micrographs in Fig. 2, FAMs are not easily discernible from the AZ61 matrix in Fig. 5(b), (c), (d), as the corrosion products appear to have masked them. A few FAMs are, however, identified and labelled as "Y" in the micrographs in Fig. 5. In addition, there are surface cracks in the syntactic samples. These cracks are related to the instability of the corrosion

https://doi.org/10.1016/j.heliyon.2019.e01531

products that are occasionally destroyed by chloride ions [28] and may be used to qualitatively assess the corrosion resistance of the syntactic foams. It is observed that there is a reduction in the prevalence of these cracks as the volume fraction of FAMs increase. This is an indication of higher corrosion resistance in the syntactic foam samples compared with the AZ61 matrix and that FAMs generally enhance the corrosion resistance of the samples. This result agrees with the corrosion rate presented in Table 2.

4. Conclusions

Lightweight AZ61/fly ash microspheres syntactic foams were successfully synthesized by powder metallurgy and microwave sintering techniques. The microstructure and electrochemical characterizations of the syntactic foams were investigated and reported. The following conclusions are derived from the results of these experimental investigations:

(1) Microwave sintering is a rapid processing technique that could be harnessed for time and energy savings, as well as minimizing the formation of interfacial reaction products in AZ61/FAMs syntactic foams.

(2) Significant weight reduction of about 23% could be achieved by incorporating fly ash microspheres into AZ61 matrix.

(3) Microstructural examination revealed that fly ash microspheres were intact, largely undamaged, and fairly distributed in the matrix of the syntactic foams.

(4) Although XRD results indicated the formation of some intermetallic phases, the absence of such phases in the microstructure suggested that microwave sintering minimised such reactions.

(5) Results from electrochemical characterization in sodium chloride solution showed that Tafel polarization curves shifted to lower current densities as the volume fraction of fly ash microspheres increased in the syntactic foams. This suggested that fly ash microspheres generally enhanced the corrosion resistance of the alloy due to the absence of a galvanic interaction between the microspheres and AZ61 matrix.

Declarations

Author contribution statement

Akeem D. Akinwekomi: Conceived and designed the experiments; Performed the experiments; Analyzed and interpreted the data; Contributed reagents, materials, analysis tools or data; Wrote the paper.

https://doi.org/10.1016/j.heliyon.2019.e01531

Funding statement

This research did not receive any specific grant from funding agencies in the public, commercial, or not-for-profit sectors.

Competing interest statement

The authors declare no conflict of interest.

Additional information

No additional information is available for this paper.

Acknowledgements

The author is grateful to Mr S Y Lau for assistance in conducting the electrochemical tests.

References

[1] A.D. Akinwekomi, C. Tang, G.C. Tsui, W. Law, L. Chen, X. Yang, M. Hamdi, Synthesis and characterisation of floatable magnesium alloy syntactic foams with hybridised cell morphology, Mater. Des. 160 (2018) 591−600.

[2] E. Aghion, Y. Perez, Effects of porosity on corrosion resistance of Mg alloy foam produced by powder metallurgy technology, Mater. Charact. 96 (2014) 78−83.

[3] A.D. Akinwekomi, W.-C. Law, M.-T. Choy, L. Chen, C.-Y. Tang, G.C.-P. Tsui, X.-S. Yang, Processing and characterisation of carbon nanotube-reinforced magnesium alloy composite foams by rapid microwave sintering, Mater. Sci. Eng. A 726 (2018) 82−92.

[4] X. Xia, J. Feng, J. Ding, K. Song, X. Chen, W. Zhao, B. Liao, B. Hur, Fabrication and characterization of closed-cell magnesium-based composite foams, Mater. Des. 74 (2015) 36−43.

[5] C.A. Vogiatzis, S.M. Skolianos, On the sintering mechanisms and microstructure of aluminium−ceramic cenospheres syntactic foams produced by powder metallurgy route, Compos. Part A Appl. Sci. Manuf. 82 (2016) 8−19.

[6] I. Orbulov, K. Májlinger, On the microstructure of ceramic hollow microspheres, Period. Polytech. Mech. Eng. 54 (2010) 89−94.

[7] A.D. Akinwekomi, W.-C. Law, C.-Y. Tang, L. Chen, C.-P. Tsui, Rapid microwave sintering of carbon nanotube-filled AZ61 magnesium alloy composites, Compos. Part B Eng. 93 (2016) 302−309.

 https://doi.org/10.1016/j.heliyon.2019.e01531

[8] A.D. Akinwekomi, M.T. Choy, W.C. Law, C.Y. Tang, Finite element modelling of CNT-filled magnesium alloy matrix composites under microwave irradiation, Mater. Sci. Forum 867 (2016) 83−87.

[9] K.N. Braszczyńska-Malik, J. Kamieniak, AZ91 magnesium matrix foam composites with fly ash cenospheres fabricated by negative pressure infiltration technique, Mater. Charact. 128 (2017) 209−216.

[10] S. Sankaranarayanan, Q.B. Nguyen, R. Shabadi, A.H. Almajid, M. Gupta, Powder metallurgy hollow fly ash cenospheres' particles reinforced magnesium composites, Powder Metall. 59 (2016) 188−196.

[11] N.N. Lu, X.J. Wang, L.L. Meng, C. Ding, W.Q. Liu, H.L. Shi, X.S. Hu, K. Wu, Electromagnetic interference shielding effectiveness of magnesium alloy-fly ash composites, J. Alloys Compd. 650 (2015) 871−877.

[12] X. Xia, X. Chen, W. Zhao, H. Xue, B. Liao, B. Hur, Z. Wang, Corrosion behavior of closed-cell AZ31 Mg alloy foam in NaCl aqueous solutions, Corros. Sci. 80 (2014) 247−256.

[13] W. Qureshi, S. Kannan, S. Vincent, N.N. Eddine, A. Muhammed, M. Gupta, R. Karthikeyan, V. Badari, Influence of silica nanospheres on corrosion behavior of magnesium matrix syntactic foam, IOP Conf. Ser. Mater. Sci. Eng. 346 (2018) 012012.

[14] G. Anbuchezhiyan, B. Mohan, D. Sathianarayanan, T. Muthuramalingam, Synthesis and characterization of hollow glass microspheres reinforced magnesium alloy matrix syntactic foam, J. Alloys Compd. 719 (2017) 125−132.

[15] Y. Bi, Y. Zheng, Y. Li, Microstructure and mechanical properties of sintered porous magnesium using polymethyl methacrylate as the space holder, Mater. Lett. 161 (2015) 583−586.

[16] J. Čapek, D. Vojtěch, Properties of porous magnesium prepared by powder metallurgy, Mater, Sci. Eng. C 33 (2013) 564−569.

[17] R.R. Zheng, Y. Wu, S.L. Liao, W.Y. Wang, W.B. Wang, A.H. Wang, Microstructure and mechanical properties of Al/(Ti,W)C composites prepared by microwave sintering, J. Alloys Compd. 590 (2014) 168−175.

[18] P.K. Rohatgi, A. Daoud, B.F. Schultz, T. Puri, Microstructure and mechanical behavior of die casting AZ91D-Fly ash cenosphere composites, Compos. Part A Appl. Sci. Manuf. 40 (2009) 883−896.

[19] C.A. Vogiatzis, A. Tsouknidas, D.T. Kountouras, S. Skolianos, Aluminum-ceramic cenospheres syntactic foams produced by powder metallurgy route, Mater. Des. 85 (2015) 444−454.

https://doi.org/10.1016/j.heliyon.2019.e01531

[20] Z. Huang, S. Yu, Microstructure characterization on the formation of in situ Mg_2Si and MgO reinforcements in AZ91D/Flyash composites, J. Alloys Compd. 509 (2011) 311−315.

[21] T. Lei, W. Tang, S. Cai, F. Feng, N. Li, On the corrosion behaviour of newly developed biodegradable Mg-based metal matrix composites produced by in situ reaction, Corros. Sci. 54 (2012) 270−277.

[22] M. Rashad, F. Pan, M. Asif, X. Chen, Corrosion behavior of magnesium-graphene composites in sodium chloride solutions, J. Magnes. Alloys 5 (2017) 271−276.

[23] M.C. Turhan, Q. Li, H. Jha, R.F. Singer, S. Virtanen, Corrosion behaviour of multiwall carbon nanotube/magnesium composites in 3.5% NaCl, Electrochim. Acta 56 (2011) 7141−7148.

[24] Q. Li, M.C. Turhan, C.A. Rottmair, R.F. Singer, S. Virtanen, Influence of MWCNT dispersion on corrosion behaviour of their Mg composites, Mater. Corros. 63 (2012) 384−387.

[25] X. Meng, D. Li, X. Shen, W. Liu, Preparation and magnetic properties of nano-Ni coated cenosphere composites, Appl. Surf. Sci. 256 (2010) 3753−3756.

[26] A. Pardo, S. Merino, M.C. Merino, I. Barroso, M. Mohedano, R. Arrabal, F. Viejo, Corrosion behaviour of silicon − carbide-particle reinforced AZ92 magnesium alloy, Corros. Sci. 51 (2009) 841−849.

[27] D. Thirumalaikumarasamy, K. Shanmugam, V. Balasubramanian, Comparison of the corrosion behaviour of AZ31B magnesium alloy under immersion test and potentiodynamic polarization test in NaCl solution, J. Magnes. Alloys 2 (2014) 36−49.

[28] M. Rashad, F. Pan, A. Tang, Y. Lu, M. Asif, S. Hussain, J. She, J. Gou, J. Mao, Effect of graphene nanoplatelets (GNPs) addition on strength and ductility of magnesium-titanium alloys, J. Magnes. Alloys 1 (2013) 242−248.

https://doi.org/10.1016/j.heliyon.2019.e01531